Building a Two-Way Hyperspectral Imaging System with Liquid Crystal Tunable Filters

Haebom Lee⋆   and   Min H. Kim⋆⋆

KAIST, Korea

Abstract. Liquid crystal tunable filters can provide rapid and vibration-less section of any wavelength in transmitting spectrum so that they have been broadly used in building multispectral or hyperspectral imaging systems. However, the spectral range of the filters is limited to a certain range, such as visible or near-infrared spectrum. In general hyperspectral imaging applications, we are therefore forced to choose a certain range of target spectrum, either visible or near-infrared for instance. Owing to the nature of polarizing optical elements, imaging systems combined with multiple tunable filters have been rarely practiced. In this paper, we therefore present our experience of building a two-way hyperspectral imaging system with liquid crystal tunable filters. The system allows us to capture hyperspectral radiance continuously from visible to near-infrared spectrum (400—1100 nm at 7 nm intervals), which is 2.3 times wider and 34 times more channels compared to a common RGB camera. We report how we handle the multiple polarizing elements to extend the spectral range of the imager with the multiple tunable filters and propose an affine-based method to register the hyperspectral image channels of each wavelength.

Keywords: hyperspectral imager, radiometric and geometric calibration

1 Introduction

Tunable filters have been broadly used to build multi- and hyperspectral imagers as they can provide rapid and vibration-less selection of any wavelength in the visible or near-infrared spectrum. Liquid crystal tunable filters (LCTFs) are efficient in changing transmittance, have therefore been preferred to build spectral imagers. Although an LCTF can provide a narrow spectral bandwidth such as 7 nm or 10 nm, its spectral coverage is limited to a certain range of visible (VIS), short-near infrared (SNIR), long-near infrared (LNIR) spectrum, etc. However, owing to the polarization nature in controlling transmittance of LCTFs, it is difficult to employ multiple LCTFs with intension to extend the spectral range of imaging systems. In this paper, we propose a simple optical design and implementation of a hyperspectral imaging system. We describe our experience about how to handle multiple polarizing elements to build a hyperspectral imager with two LCTFs of VIS and SNIR to extend the spectral range.

⋆ Author e-mail: hblee@vclab.kaist.ac.kr
⋆⋆ Corresponding author e-mail: minhkim@vclab.kaist.ac.kr

Our contributions are:

- an optical design of an hyperspectral imaging system with two LCTFs;
- radiometric and geometric calibrations for a broad range spectrum.

2 Previous Work

Hyperspectral imaging systems can be categorized into either bandpass- or dispersion-based systems. This section briefly overviews relevant previous works.

2.1 Dispersion-Based Imaging Spectroscopy

Pushbroom-Based Systems. Pushbroom-based imaging systems measure spectrum by moving the sensor along the dispersion direction. In general, the spectral resolution of such systems is determined by its optical design, i.e., the number of pixel within the spectral range measured. These systems are commonly used in air- and space-borne scanners. Beside the benefit for spectral resolution, general pushbroom systems suffer from artifacts that can exacerbate the identification of feature's composition as well as the classification of pixels. Mouroulis et al. [1] introduced a frequency-based optimization method that allows to reconstruct spatially uniform spectral information from the pushbroom systems. Recently, Hoye et al. [2] presented a pushbroom camera system by physically attaching a set of light mixing chambers to the slit.

Snapshot-Based Systems. Dispersion-based imaging systems measure a spectrum dispersed by either a diffraction grating or a prism [3]. Du et al. [4] devised a prism-based multispectral video acquisition system. Although this system provides relatively narrow bandwidth (up to 2 nm), the spatial resolution and the frame-per-second value are sacrificed in proportion. Habel et al. [5] proposed an advanced imager in terms of spectral resolution. The imager is formed with relatively cheap apparatuses while providing up to 4.89 nm spectral resolution (54 spectral bands); its spatial resolution is limited to 120 x 120 pixels. Kim et al. [6] introduced a 3D imaging spectroscopy (3DIS) system, yielding complete 3D models with hyperspectral reflectance from 369 nm to 1,003 nm at 12 nm spectral resolution.

2.2 Bandpass Filter-Based Imaging Spectroscopy

Filter-Based Systems. General bandpass filter-based imaging systems include a set of narrow bandpass filters on a wheel. These filters are used to discriminate the incident light into narrow bands. The spectral bandwidth of such systems is limited to approx. 15 nm by the bandwidth property of the filters. Rapantzikos et al. [7] implemented a bandpass-based hyperspectral imager that extracts 34 spectral bands in a range of 360—1,150 nm. Brauers et al. [8] introduced a

mathematical model for eliminating geometric distortions in multispectral images. Their multispectral system includes a set of seven bandpass filters, attached on a wheel, and yields seven multispectral images with 40 nm bandwidth. Mansouri et al. [9] integrated a multispectral camera into a 3D scanning system. The camera includes a set of seven bandpass filters and is leveled same as an LCD projector, which operates as a vertical line illumination that spans the object.

Tunable Filter-Based Systems. A tunable filter can be electronically controlled to change its spectral transmittance by applying voltage [10]. LCTFs are popularly used as they can provide the spectral resolution of the order of several nanometers with a narrow bandwidth such as ∼7 nm. Different from the pushbroom systems, the tunable filter-based systems require less computation and result in fewer artifacts than dispersion-based imaging. Attas et al. [11] also adapted an LCTF for near infrared spectroscopic imaging, and the bandwidth of the imager was 10 nm. Hardeberg et al. [12] measured the spectral reflectance of the imaged surface using an LCTF and a monochrome camera, yielding a 17-channel hyperspectral image in visible spectrum. In this paper, we propose a hyperspectral imaging system that obtains 101 spectral bands in a spectral range of 400—1,100 nm with two LCTFs of ∼7 nm bandwidth. Furthermore, the imager operates twice as fast as the previous system with help of a two-way imaging structure.

2.3 Multi-Way Imaging Systems

Beam-splitting design has been commonly used in advanced imaging systems. In general, if we split a beam into n beams, the radiative power of the beam on each sensor reduces to $1/n$ of the entering power. Wolff [13] presented a polarization camera with a beam splitter and two cameras. This seminal system can distinguish specular and diffuse reflection from metal material. Our system in particular inherits this fundamental design of two-way optics.

3 Two-Way Hyperspectral Imaging System

3.1 System Design

The fundamental optical path of our system inherits the traditional multi-way systems [13]. However, we design our optics to broaden the spectral coverage of our system by carefully choosing optical components. The arrangement of the components and the light path of our system are designed and verified with a simulation by Zemax before we build it. Incoming light enters through the first component of our system, an apochromatic objective lens (CoastalOpt UV-VIS-IR 60 mm). This lens offers focused images regardless of incident spectrum within our target range (400—1,100 nm). A FS Cooke-triplet lens with 50 mm focal length is used to collimate the focused light to make it propagate in parallel along the optical axis through the rest of our system. The parallelized beams hit the broad-band beam splitter (Spectral Optics), which transfers spectrum in between visible light and infrared light (450—1,500 nm). We locate two Varispec
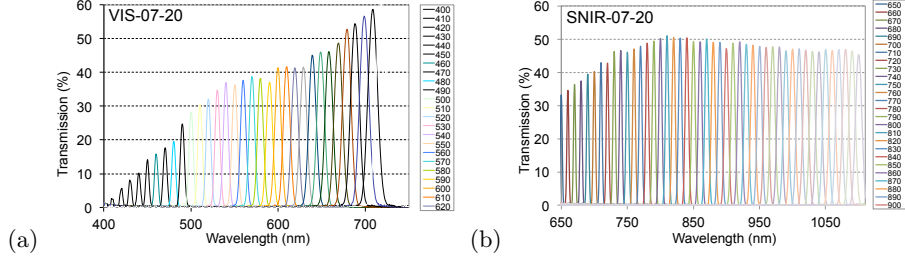
Fig. 1: *Spectral transmittance of the two LCTFs of CRi VariSpec series, employed in our imaging system. (a) VIS-07-20 visible transmittance. (b) SNIR-07-20 short near-infrared transmittance.*
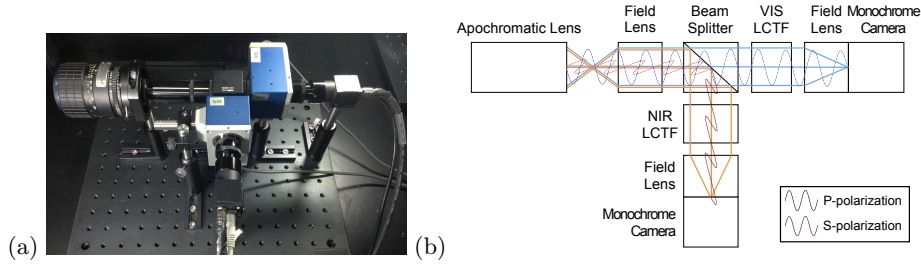

Fig. 2: *(a) Our hyperspectral imaging system and (b) its polarized light path*

LCTFs: the visible LCTF (VIS-07-20) covers spectrum range from 400 nm to 720 nm, and the infrared LCTF (SNIR-07-20) covers 650—1,100 nm, respectively along the direction of the split two-way light paths. See Fig. 1. Both LCTFs work as simple yet effective electronic narrow bandpass filter. At the end of the light path, the beams within the specified spectral range enter into a focusing lens. Finally, the intensity of the focused image is recorded via a positive triplet lens with 50 mm focal length by a monochrome camera (PointGrey FL3) on each light path. See Fig. 2 for our system and its optical design.

3.2   Polarized Light Path

Since we are set to build a hyperspectral camera, we chose a hyperspectral beam-splitter based on polarization, rather than coating. The beamsplitter polarizes the incident light as well as splits it into two ways. The light which consists of electric fields with various direction, is polarized as two direction, so-called p-polarized and s-polarized [14]. The p-polarized light means that the direction of oscillation of the light is parallel to the direction of the slit in the polarizer, whereas the s-polarized light indicates the direction is perpendicular to the slit. As the direction of the polarized light becomes different after the incident light is divided, we have to set the direction of the LCTFs perpendicular to each other as shown in Fig. 2(a). Otherwise, no image would be gained as no light passes through two polarizers. Note that we capture images with 50% of the incident light on each camera at the end of the light path via the LCTF, respectively due to the polarization-based design. Another virtue of our two-way design is that we can obtain images from both cameras simultaneously, making our system

take only 160 seconds for capturing an 101-channel hyperspectral image in total (shutter speed per shot: 1.5 seconds).

3.3   System Calibration

We then calibrated the radiometric and geometric properties of our hyperspectral imaging system for physically-meaningful measurements.

Radiometric Calibration.   The response function of our imaging system can be described as a linear product of the quantum efficiency at each wavelength Q_λ of the monochromatic sensor, the transmittance efficiency T_λ through the optical path, and the transmittance functions of two LCTFs (i.e., $F_{\text{VIS},\lambda}$ and $F_{\text{SNIR},\lambda}$). We define the camera response function $f_{\text{BAND},\lambda}$ of each filter band (of VIS and SNIR) as follows:

$$f_{\text{BAND},\lambda} = Q_\lambda T_\lambda F_{\text{BAND},\lambda} L_\lambda \ , \tag{1}$$

where L_λ is the radiance that enters to the camera system. In order to convert the raw signal levels to the incident radiance, we determine a linear transformation C_λ that describes $(Q_\lambda T_\lambda F_{\text{BAND},\lambda})^{-1}$. We measured a set of 25 training colors, including an X-rite ColorChecker and a Spectralon (calibrated to 99%) under two halogen lights. We find a linear mapping function C_λ of the raw signals that correspond to the incident radiance. The multiplication of the $f_{\text{BAND},\lambda}$ and C_λ yields the physically-meaningful radiance L_λ. See Fig. 3(a) for the training colors.

Geometric Calibration.   Although we employ an apochromatic objective lens and a set of field lenses made of Fused Silica with concern of the spectral transmittance, an incident ray refracts slightly differently according to its wavelength. This refraction effect results in forming images in different sizes per wavelength. In order to calibrate this optical geometric mismatch, we first capture a standard checker board, and for each wavelength we manually collect the image coordinates of corners. We determine an affine transform per each spectral channel A_λ to calibrate geometric distortion per wavelength. We then apply each affine transform for warping each spectral channel L_λ to the reference image (at 554 nm), yielding the hyperspectral radiance L'_λ along the wavelength axis as follow:

$$L'_\lambda = A_\lambda L_\lambda \ . \tag{2}$$

Color Calibration.   Once we capture hyperspectral radiance, we store it as a 2D float image in multi-layers in the OpenEXR format [15]. In order to present visible spectral information as a color image, we project the spectral layers L'_λ to the tristimulus values using the CIE color matching functions M_{XYZ} of 2-degree observation [16]. We then transform the tristimulus values in CIEXYZ to the sRGB color values C_{RGB} using the standard sRGB transform M_{sRGB} [17] and then apply either the gray-world white balancing algorithm [18] or the manual white balancing by manually determining the reference white in the scene:

$$C_{RGB} = M_{sRGB} M_{XYZ} L'_\lambda \ . \tag{3}$$

Finally, these color calibrated images C_{RGB} are displayed via the gamma correction (γ=2.2). See Fig. 3 for the color images that we captured with our imager.
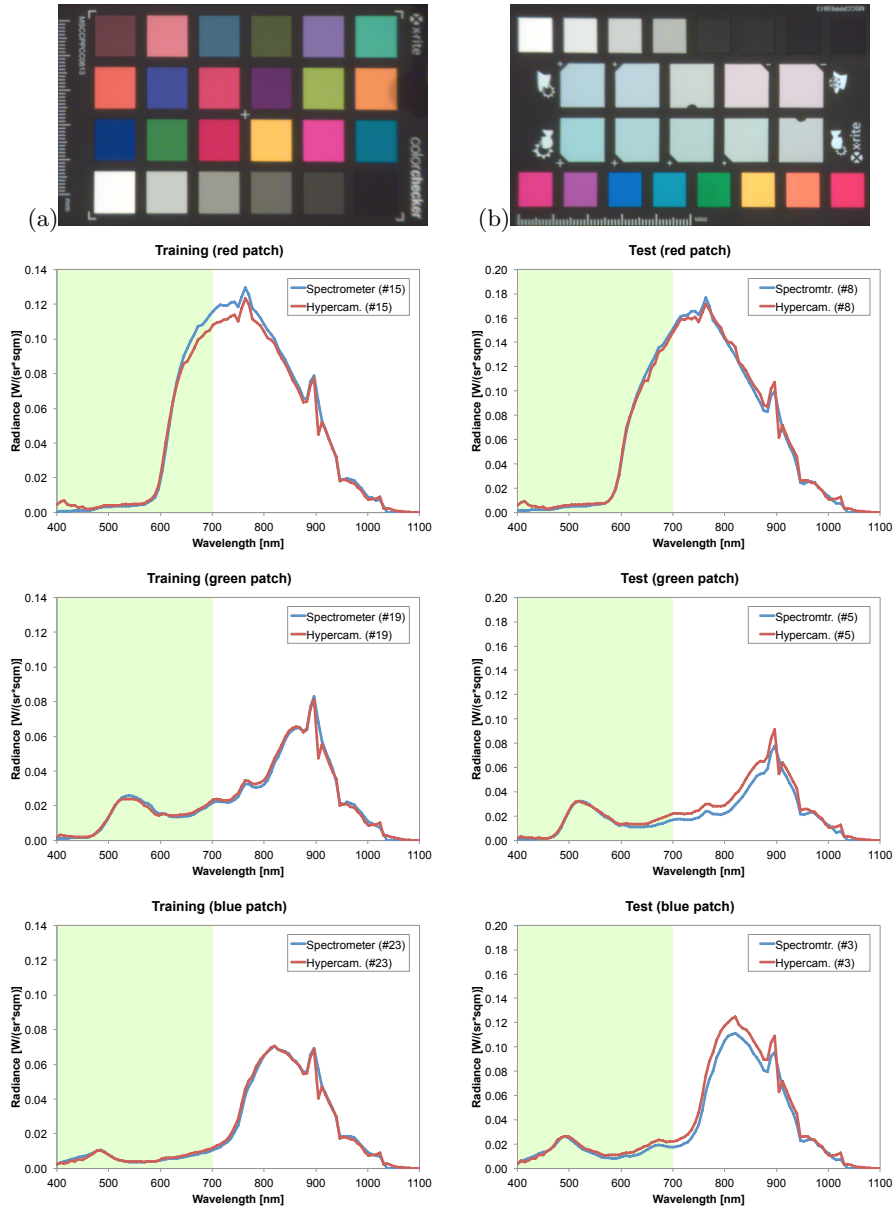
Fig. 3: *The left column (a) presents the training color patches, captured by our hyperspectral imager, followed by the radiance plots of the red, green and blue patches. The red line in the plots indicates the spectral measurement by our imager; the blue line indicates the measurement by the spectroradiometer; The green spectral region on these plots indicate the human visible spectrum. The right column (b) shows the test color patches, followed by the radiance plots of the test color patches (red, green and blue from the right).*

4   Results

4.1   Radiometric Accuracy

We compare the radiometric accuracy of our hyperspectral imager with reference measurements (measured by a calibrated hyperspectral spectroradiometer, OceanOptics USB 2000, revised for wider spectral sensitivity). See Fig. 3. Since we built a hyperspectral camera, which has twice-wider dynamic range than the human visual system, the general color difference evaluation such as CIE ΔE_{00} is not a proper evaluation standard for our system. Instead, the coefficient of variation (CV) between our hyperspectral imager and the radiometric measurements is calculated by dividing the root-mean-squared error (RMSE) by mean. The CV values on the 25 training colors and on new eight test colors are 13% and 9% (the right column on Fig. 3(b)), respectively. Fig. 4 compares the radiometric accuracy of our system with a snapshot-based hyperspectral imager (3DIS) [6], a bandpass-based hyperspectral camera (QSI 583WS) [19] and a characterized RGB camera (Nikon D100), measured on the standard ColorChecker. Our system consistently outperforms other imaging systems in terms of radiometric accuracy. In addition, the spectral resolution of our system (101 channels) is about twice as high as the 3DIS system [6] (53 channels).

4.2   Spatial Frequency

We evaluate the performance of the spatial frequency of our system by measuring the spatial frequency response (SFR) with a standard frequency target, ISO 12233 [20]. Fig. 5 compares the spatial resolution of our hyperspectral imager with a snapshot-based hyperspectral imager, 3DIS [6] in terms of the horizontal and vertical SFRs. Fig. 5(a) shows the spatial resolution in the visible spectrum, where Fig. 5(b) presents the resolution in the infrared spectrum. The spatial resolving power of our system is lower than that of the 3DIS system [6] due to the optical design of the collimating lenses and the position of the LCTFs in the optical path. Note that the spatial resolutions of both ways in our system are so close that any specific resolution of both bands is not biased in a certain axis.
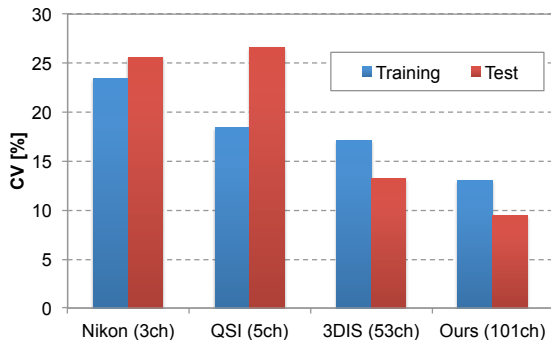

Fig. 4: *Comparison of coefficients of variation (CV) of four imaging systems: a characterized RGB camera (Nikon D100), a bandpass-based hyperspectral imager (QSI, 5 ch. [19]), a snapshot-based hyperspectral imager (3DIS, 53 ch. [6]), and our system (101 ch.).*
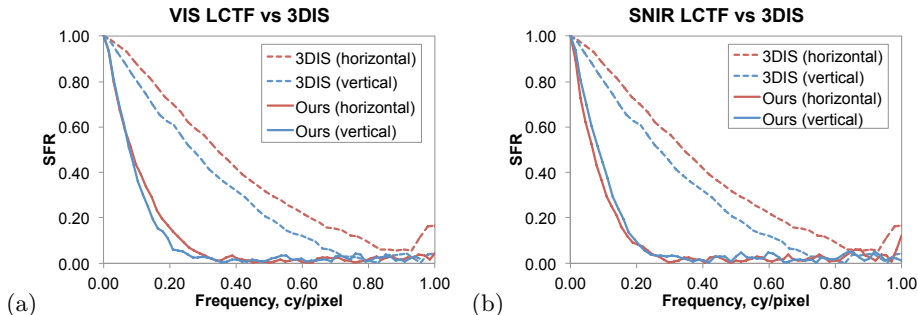
Fig. 5: *(a) presents the measured frequency response of the imager via the VIS LCTF, compared to 3DIS [6]. (b) shows the response via the SNIR LCTF.*

5   Discussion and Conclusion

We have presented a two-way hyperspectral imaging system with two LCTFs. The system allows us to measure the physically-meaningful hyperspectral radiance on static objects as the two-dimensional images based on our radiometric and geometric calibrations. We also have quantitatively evaluated our system accuracy in terms of radiometry and spatial frequency response.

Our system uses a Cooke-triplet lens to collimate the light focused by the apochromatic lens in the current system. However, the small difference between the focal length of these two lenses yields imperfect parallel beams. This difference results in insignificant blur around the edges of an image. Using multiple lenses, instead of a single Cooke-triplet, will hopefully match the focal length of the preceding lens and thus might alleviate the blur. We will resolve this issue in our future work.

Acknowledgments.

References

1. Mouroulis, P., Green, R.O., Chrien, T.G.: Design of pushbroom imaging spectrometers for optimum recovery of spectroscopic and spatial information. Applied Optics **39**(13) (2000) 2210–2220
2. Hoye, G., Fridman, A.: Mixel camera—-a new push-broom camera concept for high spatial resolution keystone-free hyperspectral imaging. Optics express **21**(9) (2013) 11057–11077
3. Vagni, F.: Survey of hyperspectral and multispectral imaging technologies. (2007)

4. Du, H., Tong, X., Cao, X., Lin, S.: A prism-based system for multispectral video acquisition. In: Computer Vision, 2009 IEEE 12th International Conference on, IEEE (2009) 175–182
5. Habel, R., Kudenov, M., Wimmer, M.: Practical spectral photography. In: Computer Graphics Forum. Volume 31., Wiley Online Library (2012) 449–458
6. Kim, M.H., Harvey, T.A., Kittle, D.S., Rushmeier, H., Dorsey, J., Prum, R.O., Brady, D.J.: 3d imaging spectroscopy for measuring hyperspectral patterns on solid objects. ACM Transactions on Graphics (Proc. SIGGRAPH 2012) **31**(4) (2012) 38:1–11
7. Rapantzikos, K., Balas, C.: Hyperspectral imaging: potential in non-destructive analysis of palimpsests. In: Image Processing, 2005. ICIP 2005. IEEE International Conference on. Volume 2., IEEE (2005) II–618
8. Brauers, J., Schulte, N., Aach, T.: Modeling and compensation of geometric distortions of multispectral cameras with optical bandpass filter wheels. In: 15th European Signal Processing Conference. Volume 15. (2007) 1902–1906
9. Mansouri, A., Lathuiliere, A., Marzani, F.S., Voisin, Y., Gouton, P.: Toward a 3d multispectral scanner: an application to multimedia. MultiMedia, IEEE **14**(1) (2007) 40–47
10. Gat, N.: Imaging spectroscopy using tunable filters: a review. In: AeroSense 2000, International Society for Optics and Photonics (2000) 50–64
11. Attas, M., Cloutis, E., Collins, C., Goltz, D., Majzels, C., Mansfield, J.R., Mantsch, H.H.: Near-infrared spectroscopic imaging in art conservation: investigation of drawing constituents. Journal of Cultural Heritage **4**(2) (2003) 127–136
12. Hardeberg, J.Y., Schmitt, F., Brettel, H.: Multispectral color image capture using a liquid crystal tunable filter. Optical engineering **41**(10) (2002) 2532–2548
13. Wolff, L.B.: Polarization camera for computer vision with a beam splitter. JOSA A **11**(11) (1994) 2935–2945
14. Hecht, E., Zajac, A.: Optics addison-wesley. Reading, Mass (1974) 301–305
15. Lucas Digital Ltd.: OpenEXR. http://www.openexr.com/ (2009)
16. CIE: Colorimetry. CIE Pub. 15.2, Commission Internationale de l'Eclairage (CIE), Vienna (1986)
17. Nielsen, M., Stokes, M.: The creation of the sRGB ICC Profile. In: Proc. Color Imaging Conf., IS&T (1998) 253–257
18. Buchsbaum, G.: A Spatial Processor Model for Object Colour Perception. J. the Franklin Institute **310**(1) (1980) 1–26
19. Kim, M.H., Rushmeier, H.: Radiometric characterization of spectral imaging for textual pigment identification. In: Proc. International Symposium on Virtual Reality, Archaeology and Cultural Heritage (VAST 2011), Tuscany, Italy, Eurographics (2011) 57–64
20. Burns, P.D., Williams, D.: Refined slanted-edge measurements for practical camera and scanner testing. In: Proc. PICS Conf., IS&T (2002) 191–195